Microscopic two-dimensional lattice model of dimer granular compaction with friction

C. Fusco,[1,*] A. Fasolino,[1] P. Gallo,[2] A. Petri,[3,4] and M. Rovere[2]

[1]*Department of Theoretical Physics, University of Nijmegen, Toernooiveld 1, 6525 ED Nijmegen, The Netherlands*
[2]*Dipartimento di Fisica, Università Roma Tre, and Istituto Nazionale per la Fisica della Materia, Unità di Ricerca Roma Tre,
Via della Vasca Navale 84, I-00146 Roma, Italy*
[3]*Consiglio Nazionale delle Ricerche, Istituto di Acustica "O. M. Corbino," Area della Ricerca di Roma Tor Vergata,
Via del Fosso del Cavaliere 100, 00133 Roma, Italy*
[4]*INFM, Unità di Roma 1, Piazzale Aldo Moro 2, 00185 Roma, Italy*

We study by Monte Carlo simulation the compaction dynamics of hard dimers in two dimensions under the action of gravity, subjected to vertical and horizontal shaking, considering also the case in which a friction force acts for horizontal displacements of the dimers. These forces are modeled by introducing effective probabilities for all kinds of moves of the particles. We analyze the dynamics for different values of the time τ during which the shaking is applied to the system and for different intensities of the forces. It turns out that the density evolution in time follows a stretched exponential behavior if τ is not very large, while a power law tail develops for larger values of τ. Moreover, in the absence of friction, a critical value τ^* exists, which signals the crossover between two different regimes: for $\tau < \tau^*$ the asymptotic density scales with a power law of τ, while for $\tau > \tau^*$ it reaches logarithmically a maximal saturation value. Such behavior smears out when a finite friction force is present. In this situation the dynamics is slower and lower asymptotic densities are attained. In particular, for significant friction forces, the final density decreases linearly with the friction coefficient. We also compare the frictionless single tap dynamics to the sequential tapping dynamics, observing in the latter case an inverse logarithmic behavior of the density evolution, as found in the experiments.

I. INTRODUCTION

The process of compaction in granular media attracts a great deal of attention in the scientific community, in particular amongst physicists and chemical engineers. In fact it displays features that are general enough to make it suitable for investigation through models that are relatively simple, at least for a nonequilibrium process. Granular compaction therefore appears appealing for testing new promising and unifying ideas in the field of disordered systems [1–4].

Grains poured into a vessel fill it with loose arrangements and relatively low densities. The action of external perturbations, such as shaking and tapping, in the presence of an external driving, such as the gravity field, leads to a very slow increase of density through a rich phenomenology, displaying different regimes and both reversible and irreversible dynamical phases [5–18]. A number of different lattice models have been recently investigated in order to unravel the microscopic mechanisms producing such behaviors, and to clarify to which extent they may be considered general, also in relation to other disordered systems such as glasses [19–27].

In this work we introduce a lattice gas model for dimer compaction which includes, besides the vertical, also horizontal shaking and friction. Friction, although playing a fundamental role in real granular systems, has not been introduced so far in models for compaction. Horizontal shaking has been considered only experimentally for non-Brownian

spheres where it seems to favor local dense crystalline order [28,29]. Highly anisotropic granulars, namely, rods, have been recently investigated under vertical shaking. In contrast to sphere packings which tend to end up in disordered configurations, evidence is found that the particle anisotropy drives ordering [30]. We try to incorporate in our model, albeit in a simplified manner, all these aspects, namely, particle anisotropy, horizontal shaking, and frictional dynamics, which we find to affect the compaction process significantly.

In particular, our model is based on the diffusional dynamics of dimers, considered as rigid and nonoverlapping particles, which occupy two lattice sites on a square lattice. The model has no quenched disorder, but for this type of dynamics glasslike properties may be expected [31], because of the onset of geometrically frustrated configurations. Since the number of states with the closest packed density is exponentially large in the lattice size [32,33], this model is intrinsically different from the other lattice models recently investigated [19–25] and is suitable to understand how horizontal shaking and friction may influence the general characteristics attributed to the compaction process.

In the following section we describe in detail the model and the Monte Carlo method that we used. In Sec. III we discuss the results for the compaction dynamics without friction and illustrate the evolution of the packing structure. In Sec. IV we introduce the effect of friction and show its crucial role in the dynamical behavior. The final section is devoted to the conclusions.

II. MODEL

We consider a square lattice of $N = L \times L$ sites, with lateral periodic boundary conditions, an open boundary at the

---

*Author to whom correspondence should be addressed. Electronic address: fusco@sci.kun.nl
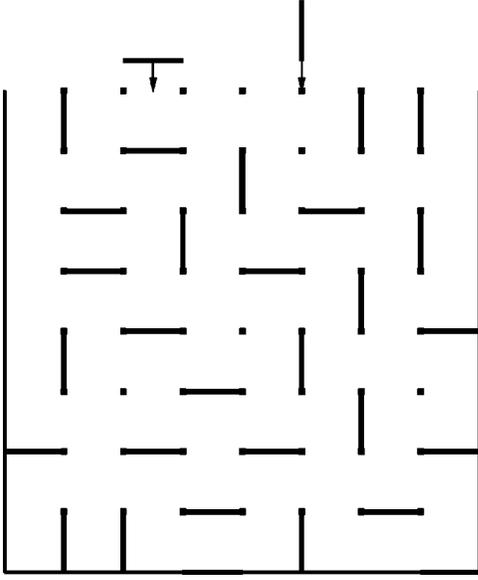
FIG. 1. Schematic picture of the lattice model studied. The arrangement of the particles is the result of the initial sample preparation. Note that lateral periodic boundary conditions have been imposed.

top, and a rigid wall at the bottom. Elongated particles occupying two consecutive lattice sites (dimers) are inserted from the top one at the time with random (horizontal or vertical) orientation, letting them fall down keeping their orientation fixed, until reaching a stable position. In this way we are able to prepare the system in an initial state which is saturated, i.e., no more particles can be put in, and with statistically reproducible density ρ_0, i.e., characterized by a precise mean value, $\rho_0 \simeq 0.587$, corresponding to a random loose packing. In the present model, particles are subjected only to geometrical interactions, and the nonoverlapping condition produces strong constraints on their relative positions (see Fig. 1). The aim of this paper is to study the system in the presence of gravity and external vibrations, with the possibility of taking into account also a frictionlike force for horizontal displacements. For this purpose we perform Monte Carlo (MC) simulations introducing a random diffusive dynamics in our model, which mimics the aforementioned forces and preserves the geometrical constraints. At this stage, we consider separately horizontal and vertical dimers and keep their orientation fixed without allowing rotations. We plan to introduce this feature, which would make the model more realistic in the future. We consider in detail a single tap applied to the system for a fixed time τ, comparing it with the multiple tapping for selected cases (see [19]). We first describe the dynamics without friction. The dynamics can be divided into two stages: (i) for $t<\tau$ particles can move horizontally (left or right with probability $p_h/2$) and vertically (upwards with probability p_{up} or downwards with probability p_{down}); (ii) for $t>\tau$ only downward movement of particles is possible (i.e., $p_{up}=p_h=0$ and $p_{down}=1$). We note that τ^{-1} can be thought of as the quench rate of an initially annealed system. The probabilities for the different moves are normalized: $p_h+p_{up}+p_{down}=1$. Physically p_{down} corresponds to

the action of gravity, while p_h and p_{up} represent, respectively, the horizontal and vertical component of the external tap. The functional form chosen for the time dependence of p_h and p_{up} is [19]

$$p_h(t)=p_h^0(1-t/\tau)\theta(\tau-t), \tag{1}$$

where $\theta(x)$ is the Heaviside function [the same expression holds for $p_{up}(t)$, with p_{up}^0 instead of p_h^0]. $p_{down}(t)$ is determined from the normalization condition

$$p_{down}(t)=1-p_{up}(t)-p_h(t)=p_{down}^0+(p_{up}^0+p_h^0)t/\tau, \tag{2}$$

where $p_{down}^0 \equiv 1-(p_{up}^0+p_h^0)$. Since $p_{down}(t) \geq 0 \; \forall \, t$ it must be $p_{up}^0+p_{down}^0 \leq 1$. If not stated explicitly otherwise, we assume $p_{down}^0=p_{up}^0$, so p_h^0 results to be $p_h^0=1-2p_{up}^0$, that is only one independent input parameter is needed. In each MC move one extracts a particle with uniform probability, chooses a move for this particle according to the values of p_h, p_{up}, and p_{down}, and performs the move if all the geometrical constraints are satisfied. One MC time step (MCS) corresponds to N attempted moves. In the following, time is always given in units of MCS. To save CPU time we used an algorithm in which the attempted moves are always successful, and consistently updated time through probabilistic arguments (for the details of our computation see Ref. [34] on a reaction-diffusion model for dimers). We performed our MC simulations on a lattice with $L=100$, for which we checked that finite size effects are negligible.

As a next step we introduce friction between adjacent horizontal layers in the material in the following simplified way: the effective probability of making a horizontal move is set to

$$
\begin{aligned}
p_h^{eff}(t) &= p_h(t)-\mu[p_{down}(t)-p_{up}(t)] \\
&= [p_h^0-\mu(1-p_h^0-2p_{up}^0)-[p_h^0+\mu(p_h^0+2p_{up}^0)] \\
&\quad \times t/\tau]\theta(t_0(\mu)-t), \tag{3}
\end{aligned}
$$

where

$$t_0(\mu)=\tau\left[\frac{p_h^0-\mu(1-p_h^0-2p_{up}^0)}{p_h^0+\mu(p_h^0+2p_{up}^0)}\right], \tag{4}$$

μ acts as a friction coefficient ($\mu>0$) and the "friction force" is proportional to the load, represented by the net vertical force, reducing the probability of the move. This assumption implies that the frictional force occurs only for horizontal moves, independently of whether an underlying dimer (i.e., a dimer in the adjacent lower row) is present. We are aware that this is a simplified approximation, but it is meant as a first step in describing this complex process. To ensure $p_h^{eff} \geq 0$ at $t=0$, μ has to satisfy the condition

$$\mu \leq \frac{p_h^0}{(1-p_h^0-2p_{up}^0)}.$$
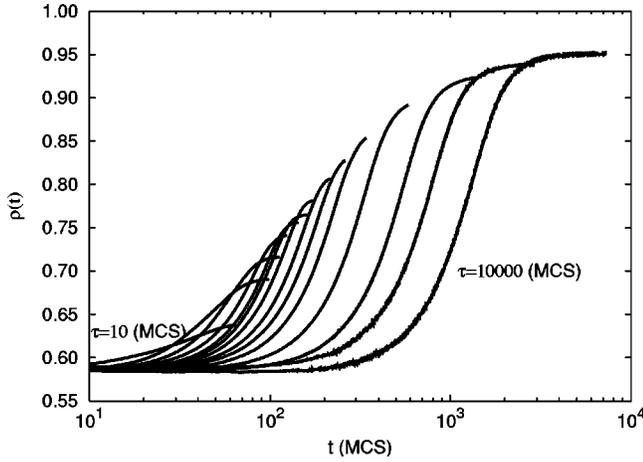
FIG. 2. Temporal behavior of density in the frictionless case for different values of the shaking time τ (from left to right $\tau = 10, 30, 50, 80, 103, 125, 150, 210, 280, 400, 800, 2000, 4000, 10\,000$). The horizontal shaking amplitude is $p_h^0 = 0.1$.

In addition, for the friction force to give a negative contribution to p_h, one must have $p_{down}(t) \geq p_{up}(t) \; \forall \; t$ (this is automatically satisfied with our choice $p_{down}^0 = p_{up}^0$). Note that the normalization of the frictionless probabilities is still $p_{up} + p_{down} + p_h = 1$. In other terms we have introduced a "sticking" probability (probability that the particle does not move) p_s, given by $p_s = \mu(p_{down} - p_{up})$. If we put $\mu = 0$ we recover the frictionless case.

III. COMPACTION DYNAMICS WITHOUT FRICTION

We have analyzed the time behavior of the mean density of the system $\rho(t)$ (number of occupied sites normalized to the total number of sites) by measuring it in the lower 30% of the box at time t. In this way we are sure to measure density at the bulk, since fluctuations can increase significantly in the proximity of the open boundary, resulting in a quite complicated compaction behavior in this region [23]. Since the statistical fluctuations of the density can be quite relevant, we have performed several MC realizations (up to 500) of the process in order to obtain reliable results. After preparing the system in its low density configuration [$\rho_0 \equiv \rho(t=0) \simeq 0.587$], the diffusive dynamics starts as described in the preceding section. p_h^0 is chosen as an input parameter and consequently $p_{up}^0 = p_{down}^0 = (1 - p_h^0)/2$. We stop the simulations when a steady asymptotic value ρ_∞ of the density is reached. We have studied the density evolution for different values of p_h^0 and of the shaking time τ, in order to find out if some kind of scaling law, describing the behavior of the final density as a function of these parameters, exists. As far as we know, no systematic study concerning this point has been performed.

The time behavior of the density for several choices of τ is illustrated in Fig. 2, where a relatively low value of p_h^0 has been used ($p_h^0 = 0.1$). We have observed that the dynamics gets drastically slower when τ increases; actually, because of our shaking rule, Eq. (1), when a long tap is applied the density does not significantly change in the initial steps of
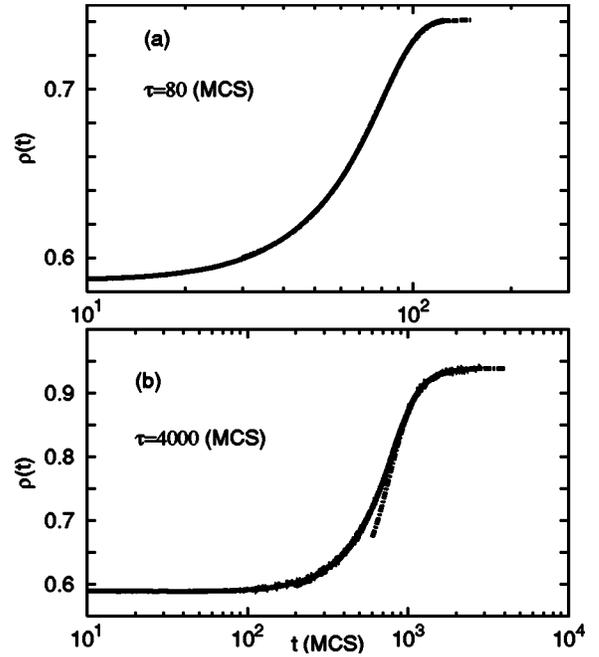
FIG. 3. Density relaxation in the frictionless case for $\tau = 80$ (a) and $\tau = 4000$ (b). The solid lines are the result of the MC simulation, the dashed lines are stretched exponential fits using Eq. (5) for $\rho(t) \geq 0.6$, with parameters $C \simeq 1.1$, $t_0 \simeq 170$, $\tau_0 \simeq 250$, $\beta \simeq 9.8$ for $\tau = 80$ (a), and $C \simeq 1.1$, $t_0 \simeq 2900$, $\tau_0 \simeq 3600$, $\beta \simeq 9.7$ for $\tau = 4000$ (b). The dot-dashed line in (b) is a fit for $t \geq 1000$ according to Eq. (6) with parameters $B \simeq 0.018$, $\tau \simeq 330$, and $\alpha \simeq 4.95$. The horizontal shaking amplitude is $p_h^0 = 0.1$.

the process, but the evolution takes place on a much wider time scale and finally a larger value of the asymptotic density is achieved. We have tried to fit different functional forms to the data in Fig. 2, looking in particular at the relaxation functions proposed in the seminal experimental paper of Ref. [5]. It is clear that the observed dynamical behavior is very complex and is not compatible with a single relaxation time, i.e., a simple exponential. We have found that the commonly claimed inverse logarithmic relaxation does not hold for our system in the single tap case. Instead, the most suitable functional form for our data is a stretched exponential, as proposed by Nicodemi *et al.* [19] for the single tapping dynamics:

$$\rho(t; \tau, p_h^0) = \rho_\infty(\tau, p_h^0) - C[\rho_\infty(\tau, p_h^0) - \rho_0]$$
$$\times \exp\{-[(t+t_0)/\tau_0]^\beta\}, \qquad (5)$$

where the fit parameters C, t_0, τ_0, and β depend in principle on both τ and p_h^0. Actually, it turns out from our fits that $C \simeq 1.1$ and $\beta \simeq 10$ are almost independent of τ and p_h^0. In Fig. 3(a) we show the density evolution for a small value of τ. As can be seen, the intermediate-long time behavior can be accurately fitted by Eq. (5) (all fits have been performed for $\rho \geq 0.6$). As τ increases, however, Eq. (5) fails to reproduce the long time regime. In fact, a power law tail develops, indicating that the compaction process slows down at long
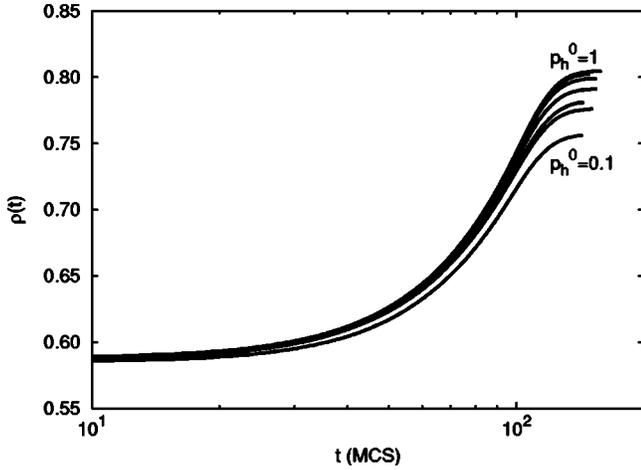
FIG. 4. Temporal behavior of density in the frictionless case for different values of the horizontal shaking amplitude p_h^0 (from bottom to top $p_h^0 = 0.1, 0.2, 0.3, 0.4, 0.6, 0.8, 1$). The shaking time is $\tau = 103$.

FIG. 5. Temporal behavior of density in the frictionless case for different values of the ratio p_{up}^0/p_{down}^0: $p_{up}^0/p_{down}^0 = 1$ (solid line), $p_{up}^0/p_{down}^0 = 2$ (dashed line), and $p_{up}^0/p_{down}^0 = 3$ (dotted line). The shaking time is $\tau = 80$ and the horizontal shaking amplitude is $p_h^0 = 0.1$.

times for large shaking duration. The fitting function that we have used for the long time behavior is

$$\rho(t; \tau, p_h^0) = \rho_\infty(\tau, p_h^0) - \frac{\rho_\infty(\tau, p_h^0) - \rho_0}{1 + B(t/\tau_0')^\alpha}. \quad (6)$$

This is illustrated in Fig. 3(b) for $\tau = 4000$. Fit (6) has been applied for $\tau > 1000$. The exponent α of this power law can be considered independent of τ ($\alpha \simeq 5$). However, the stretched exponential function still describes the density behavior in the intermediate time regime well.

We have also studied the density relaxation for different values of p_h^0 at fixed τ ($\tau = 103$). The corresponding plots are shown in Fig. 4, where it is clear that the role of the horizontal shaking amplitude is crucial in determining the asymptotic density.

Moreover, we have considered the effect of different ratios p_{up}^0/p_{down}^0 on the density evolution, which we show in Fig. 5. When $p_{up}^0 > p_{down}^0$ we observe a decompaction at the beginning of the process, which becomes more pronounced if the vertical tap is stronger. This reflects the fact that, in the

initial transient, the density decreases at the bottom of the container for a strong tap. Such a decompaction upon vertical acceleration increase seems to be a genuine feature of two-dimensional systems, as claimed in [35]. The saturation density is also sensitive to variations of p_{up}^0 and decreases for increasing p_{up}^0/p_{down}^0. However, the scaling behavior does not change and the density evolution can still be described by Eq. (5), but with a smaller value of β with respect to the case $p_{up}^0 = p_{down}^0$ ($\beta \simeq 9.8$ for $p_{up}^0/p_{down}^0 = 1$, $\beta \simeq 7.6$ for $p_{up}^0/p_{down}^0 = 2$, and $\beta \simeq 6.5$ for $p_{up}^0/p_{down}^0 = 3$).

In order to gain a better understanding of the degree of compaction of the system, we investigated the dependence of the saturation density ρ_∞ on τ and p_h^0. The data for ρ_∞ vs τ are plotted in Fig. 6(a). A crossover from a power law scaling to a logarithmic behavior is observed at a characteristic value $\tau^* \simeq 200$:

$$\rho_\infty(\tau) = (\tau/\tau_l)^\delta \quad \text{for} \quad \tau < \tau^*,$$

$$\rho_\infty(\tau) = \rho_m - B/\ln(\tau/\tau_r) \quad \text{for} \quad \tau > \tau^*, \quad (7)$$
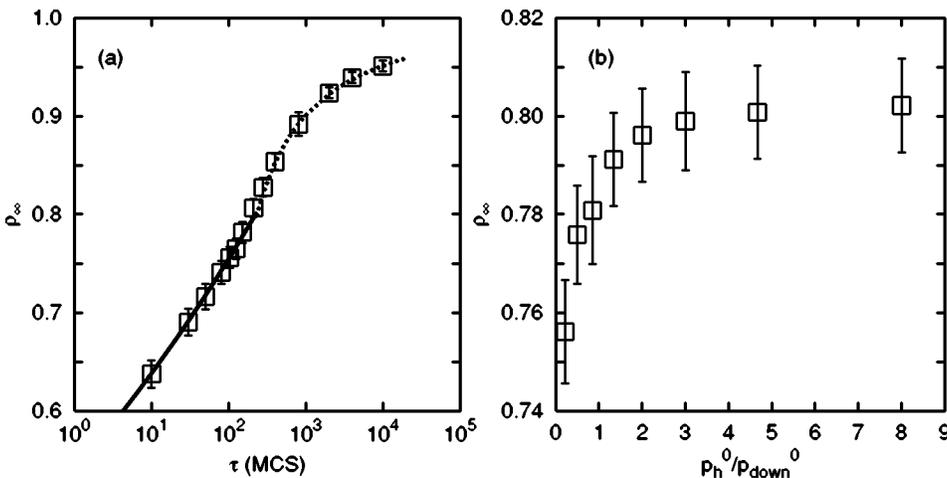
FIG. 6. Saturation density ρ_∞ in the frictionless case as a function of the shaking time τ (a) and the ratio p_h^0/p_{down}^0 (b). The squares are the numerical data, while the solid line and dotted line in (a) are, respectively, the fits for $\tau < \tau^*$ and $\tau > \tau^*$ given in Eq. (7). The horizontal shaking amplitude in (a) is $p_h^0 = 0.1$ and the shaking time in (b) is $\tau = 103$.
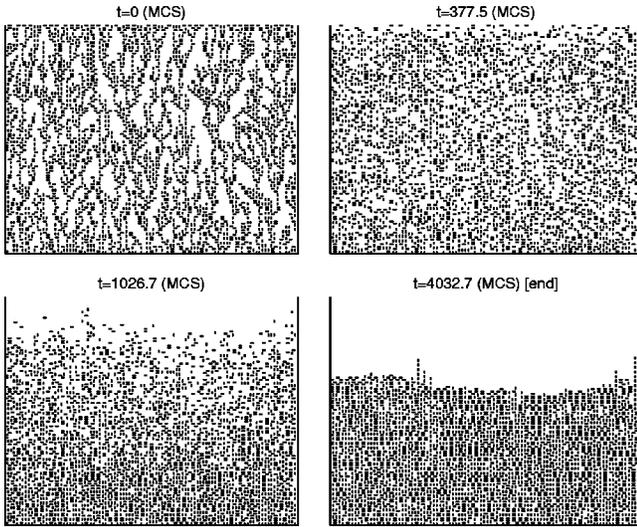
FIG. 7. Snapshots of one particular realization of the packing at different times for $\tau=4000$. The horizontal shaking amplitude is $p_h^0=0.1$.

FIG. 8. Snapshots of the final configuration of the packing for two different p_h^0 and fixed τ (upper part) and two different τ and fixed p_h^0 (lower part).

where $\tau_l \simeq 4.5 \times 10^3$, $\delta \simeq 0.073$, $\rho_m \simeq 1$, $B \simeq 0.6$, and $\tau_r \simeq 18$. This means that for large values of τ the process gets slower and slower, as observed before, eventually reaching a final value of the density $\rho_m \simeq 1$ for $\tau \to \infty$ (which corresponds to about the maximal density for the system [34]). The variation of ρ_∞ with respect to the ratio p_h^0/p_{down}^0 is illustrated in Fig. 6(b). The increase of ρ_∞ is more pronounced for low values of p_h^0, while it tends to saturate afterwards. This compares qualitatively well to the experimental results for a horizontally shaken box filled with beads [28], where it was found that for low filling rates the packing crystallizes upon increase of the adimensional parameter $\Gamma = A\omega^2/g$ (where A and ω are the amplitude and pulsation of the vibration and g is the gravitational acceleration), which roughly corresponds to p_h^0/p_{down}^0.

In Fig. 7 we show some snapshots of one particular realization of the compaction process for $\tau=4000$. We see how the packing evolves from a highly disordered state at $t=0$ to a polycrystalline state, made of many crystalline ordered domains, at the end of the compaction. As time increases the

order proceeds from the bottom to the top of the packing while empty spaces reduce in size. The final state is therefore characterized by the presence of large clusters of horizontal and vertical dimers. In order to demonstrate that the shaking amplitude p_h^0 and time τ play a significant role, we have reported in Fig. 8 a comparison between the final configurations for $p_h^0=0.1$ and $p_h^0=0.8$ at fixed $\tau=103$ (upper part), and for $\tau=80$ and $\tau=4000$ at fixed $p_h^0=0.1$ (lower part). We notice that an intense or/and long tap is effective in locally removing frozen configurations through collective rearrangements of particles, thus letting the defects migrate towards the free surface of the packing.

We have also investigated in detail the behavior of the parameters of the stretched exponential fit [Eq. (5)] t_0 and τ_0, which is reported in Fig. 9. We have observed a change of behavior in correspondence to the critical value of the shaking time τ^*, the same value determining the change in the behavior of ρ_∞ vs τ described in Eq. (7). A similar transition was also signaled by Nicodemi *et al.* [19]. The parameters of the stretched exponential relaxation Eq. (5) change according to
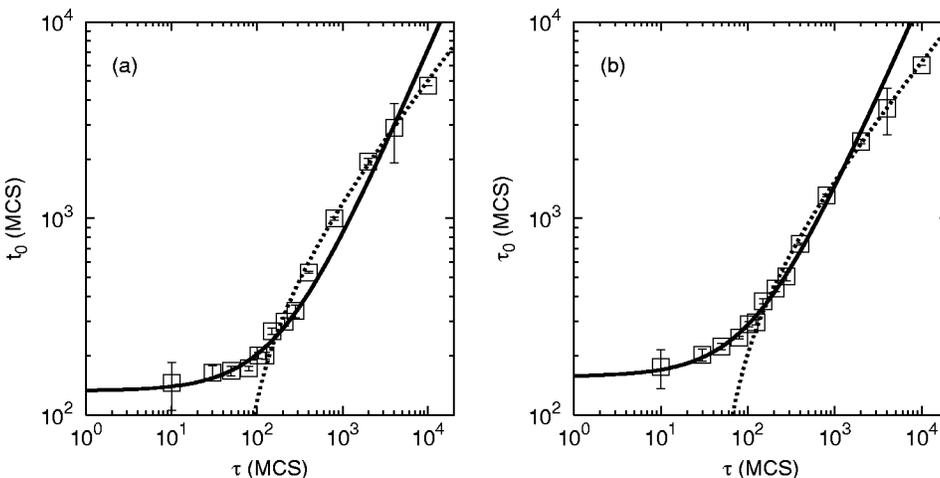
FIG. 9. Parameters t_0 (a) and τ_0 (b) of fit Eq. (5) in the frictionless case. The squares are the numerical data, while the solid line ($\tau < \tau^*$) and dotted line ($\tau > \tau^*$) in (a) are the functions given in Eq. (8) and those in (b) are the functions given by Eq. (9). The horizontal shaking amplitude is $p_h^0=0.1$.
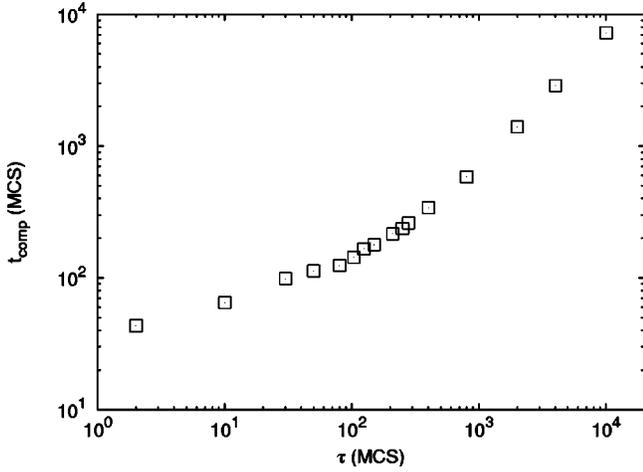
FIG. 10. Compaction time t_{comp} vs shaking time τ in the frictionless case. The horizontal shaking amplitude is $p_h^0 = 0.1$.

$$t_0(\tau) = \tau/t_1 + t_< \quad \text{for} \quad \tau < \tau^*,$$

$$t_0(\tau) = (\tau/t_2)^\gamma + a \quad \text{for} \quad \tau > \tau^*, \quad (8)$$

$$\tau_0(\tau) = \tau/\tau_1 + \tau_< \quad \text{for} \quad \tau < \tau^*,$$

$$\tau_0(\tau) = (\tau/\tau_2)^\gamma + b \quad \text{for} \quad \tau > \tau^*, \quad (9)$$

where $t_1 \simeq 1.40$, $t_< \simeq 130$, $t_2 \simeq 7 \times 10^{-5}$, $\gamma \simeq 0.47$, $a \simeq -700$, $\tau_1 \simeq 0.76$, $\tau_< \simeq 150$, $\tau_2 \simeq 10^{-4}$, $b \simeq -700$. It is remarkable that both t_0 and τ_0 vary linearly with τ for $\tau < \tau^*$ and both follow a power law with the same exponent γ

for $\tau > \tau^*$. This could mean that they are both determined by the same relaxation mechanism as τ changes [i.e., if we define $\bar{t}_0 = t_0 - t_<$, $\bar{\tau}_0 = \tau_0 - \tau_<$, $\tilde{t}_0 = t_0 - a$, and $\tilde{\tau}_0 = \tau_0 - b$, we see from Eqs. (8) and (9) that $\bar{t}_0/\bar{\tau}_0$ and $\tilde{t}_0/\tilde{\tau}_0$ are constants independent of τ].

We note that the critical shaking time τ^* physically signals the crossover between two different regimes. In fact, a careful inspection of Fig. 2 shows that, for $\tau < \tau^*$, compaction occurs after the shaking (when $p_h = p_{up} = 0$ and $p_{down} = 1$) and is mainly driven by gravity. On the other hand, when $\tau > \tau^*$, the compaction time (t_{comp}), i.e., the time needed to reach the saturation density, is shorter than τ, and vibrations act on the system till the end of the process (see Fig. 10). We believe this is responsible for the power law tail for large values of τ, since the combined action of shaking and gravity produces a slowing down of the dynamics, enabling at the same time to obtain denser packings. However, we are not sure whether this picture corresponds to a real dynamical phase transition in the system, and, moreover, the identification of an order parameter would be quite problematic. Therefore a deeper investigation on this point is needed and we hope to stimulate some future experimental and theoretical works.

Now we briefly mention the main changes occurring when a sequential tapping is applied to the system. Although the single tap dynamics can give an insight into the dynamical evolution and the relaxation of the system, the sequential tapping procedure can be closely related to experimental situations. In Fig. 11(a) we compare the density evolution obtained by a single tap of duration $\tau = 10\,000$ with that obtained by a sequential tapping applied for the same amount of time τ. In particular, we have generated 5000 taps, each of which was applied for a time $\tau/5000$. From the comparison we deduce that the multiple tapping dynamics is slower, suggesting that the fitting form Eq. (5) cannot describe properly the density evolution in this case. Besides, the saturation density is also lower. In Fig. 11(b) we characterize more
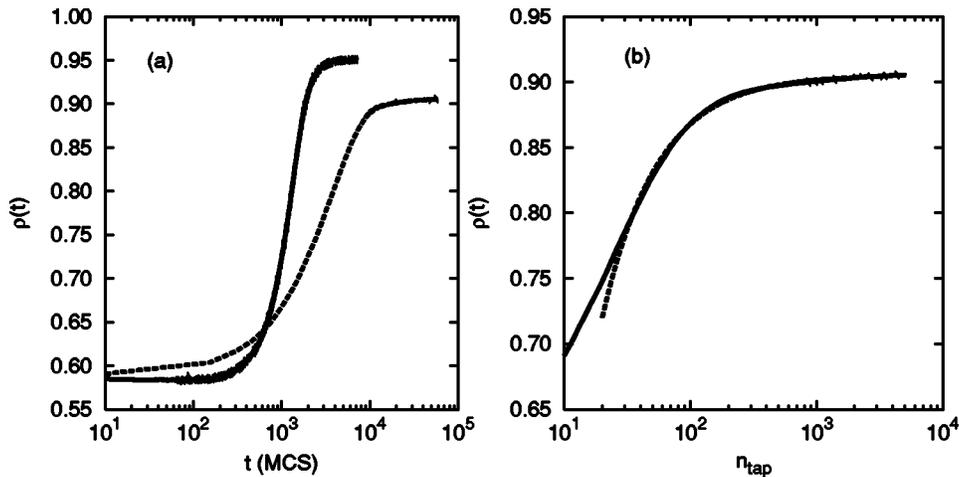
FIG. 11. Comparison between single and multiple tapping. In (a) the behavior of density as a function of time is plotted: the solid line is obtained by a single tap with $\tau = 10\,000$, while the dashed line is the result of 5000 taps, each of which is applied for a time $\tau/5000$. In (b) the density is shown as a function of the number of taps (n_{tap}): the solid line is the result of the simulation and the dashed line is a fit according to Eq. (10) for $n_{tap} > 40$, with parameters $c \simeq 47$, $d \simeq 1.2 \times 10^5$, and $T \simeq 3 \times 10^4$. The horizontal shaking amplitude is $p_h^0 = 0.1$.
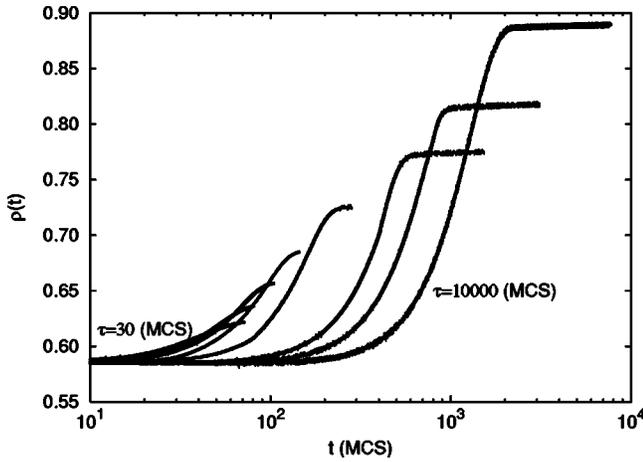
FIG. 12. Temporal behavior of density for friction coefficient $\mu=0.4$ and different values of the shaking time τ (from left to right $\tau=30,50,80,150,400,2000,4000,10\,000$). The horizontal shaking amplitude is $p_h^0=0.1$.

FIG. 13. Density relaxation for $\mu=0$ (top solid line) and $\mu=0.4$ (bottom solid line). The dashed lines are stretched exponential fits using Eq. (5) for $\rho(t)\geq0.6$, with parameters $C\simeq1.1$, $t_0\simeq275$, $\tau_0\simeq400$, $\beta\simeq9$ for $\mu=0.4$ (the parameters for $\mu=0$ can be found in the caption of Fig. 3). We note that the major differences between the two curves are due to the different values of β and ρ_∞ [$\rho_\infty(\mu=0)\simeq0.782$ and $\rho_\infty(\mu=0.4)\simeq0.685$]. The horizontal shaking amplitude is $p_h^0=0.1$ and the shaking time is $\tau=80$.

quantitatively the dynamical behavior by plotting the density as a function of the number of taps. It turns out that in this case the intermediate-long time evolution of the density can be described by the claimed inverse logarithmic law, which was also found in the experiments [5]:

$$\rho(t)=\rho_\infty-c\,\frac{\rho_\infty-\rho_0}{1+d\ln(1+t/T)}.\tag{10}$$

In this way we can connect directly our model to the experimental data and we can also examine the effect of different dynamical shaking procedures on the compaction process. In this respect, our results are in agreement with those of Nicodemi *et al.* [19], who find a similar change of behavior when considering single and multiple tapping. This should clarify to a certain extent the mechanisms of density relaxation in different dynamical situations.

IV. COMPACTION DYNAMICS WITH FRICTION

When a frictional force is introduced, as described in Sec. I, some qualitative and quantitative changes are found. In

Fig. 12 the time evolution of the density for a fixed value of the friction coefficient μ and several choices of τ is displayed. A comparison with Fig. 2 shows that for a same value of τ a much smaller asymptotic density is reached, and that a slowing down of the dynamical behavior occurs. As a consequence, larger values of τ are needed to obtain the same final densities as for $\mu=0$. In Fig. 13 a comparison of $\rho(t)$ between $\mu=0$ and $\mu=0.4$ for $\tau=80$ is illustrated. It seems that the same functional form Eq. (5) adopted for $\mu=0$ can be used to describe the dynamical evolution of the system. In spite of that, for $\mu\neq0$ some slight discrepancies in the tails can be detected for small values of τ, not visible at the level of detail of the figure. This means that the reduced probability for horizontal moves affects the compaction mainly in the late stages of the process.

We have also examined the μ dependence of $\rho(t)$. The curve for $\mu=0$ is far above the others, and furthermore the
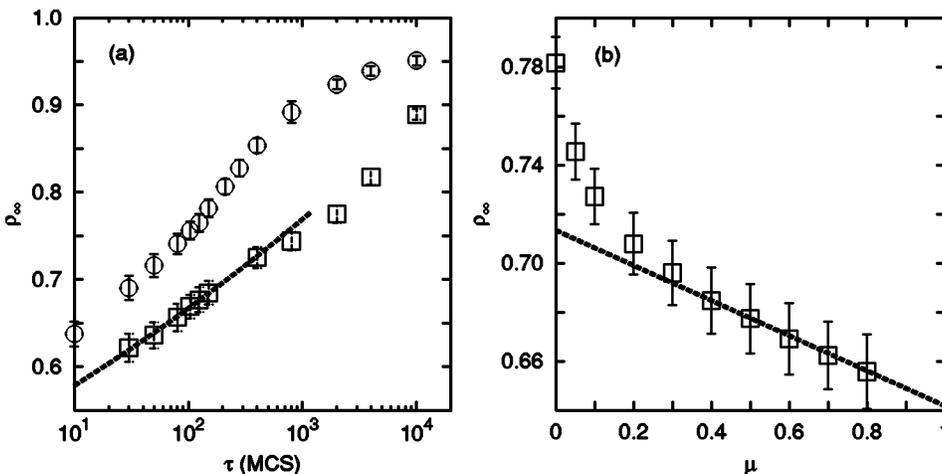
FIG. 14. Saturation density ρ_∞ as a function of (a) τ for $\mu=0.4$ and (b) of μ for $\tau=150$. The circles in (a) and the squares in (a) and (b) are the numerical data for $\mu=0$ and $\mu=0.4$, respectively. The dashed lines in (a) and (b) are fits, respectively, according to Eqs. (11) and (12). The horizontal shaking amplitude is $p_h^0=0.1$.
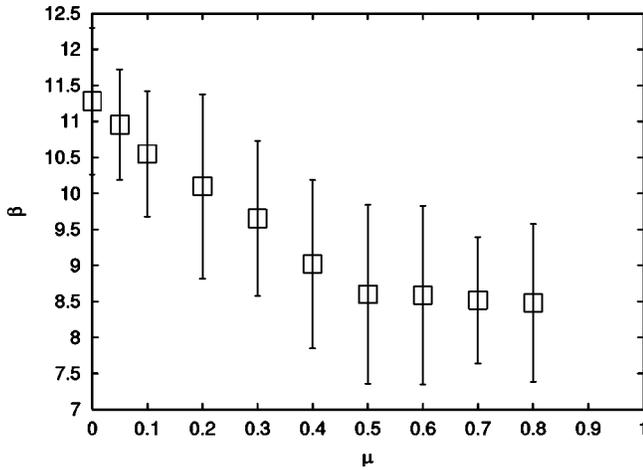
FIG. 15. Stretched exponent β of Eq. (5) vs friction coefficient μ for $p_h^0 = 0.1$ and $\tau = 150$.

difference between the curves for low values of μ is more marked. Such differences show up only after an initial transient in which the various curves are practically superimposed one on the others (the curves do not start diverging significantly until the density reaches about 0.6). This is in compliance with what we have just said about the effectiveness of friction in the asymptotic dynamics.

The behavior of the asymptotic density is depicted in Fig. 14 and reveals more interesting aspects. In Fig. 14(a) we have plotted $\rho_\infty(\tau)$ for $\mu = 0$ and $\mu = 0.4$. We were able to identify a power law regime for small τ also for $\mu = 0.4$:

$$\rho_\infty(\tau) = (\tau/\tau_l^{(\mu)})^{\delta^{(\mu)}} \qquad (11)$$

with $\delta^{(\mu)} \simeq 0.062$ [not very different from δ in Eq. (7)] and $\tau_l^{(\mu)} \simeq 6.9 \times 10^4$. Thus, saturation density scales in the same way as for $\mu = 0$, with nearly the same exponent but with a very different relaxation time (more than one order of magnitude larger), i.e., the process is much more sluggish. We did not manage to find the functional behavior for larger τ and it is not very clear whether it is possible to define a crossover shaking time, at least for the values of τ we have considered. For $\tau > 1000$, ρ_∞ increases more steeply than for $\mu = 0$ and it is likely that one could find another regime for larger τ. However computational limitations prevented us to explore in detail the region for $\tau > 10000$ (since simulations become more and more time consuming as τ increases), and we will address this problem in the future.

Finally in Fig. 14(b) we have analyzed the behavior of ρ_∞ vs μ. Interestingly, ρ_∞ decreases linearly with μ for $\mu > 0.4$:

$$\rho_\infty(\mu) = A - B\mu, \qquad (12)$$

where $A \simeq 0.71$ and $B \simeq 0.073$. Instead the decrease is more drastic for lower values of μ, as noted above. This fact

might indicate a change of behavior in the dynamics of the system as a function of the friction coefficient. For this purpose we show in Fig. 15 the stretched exponent β of Eq. (5) vs μ. It rapidly decreases for $\mu < 0.4$, but it is almost constant for larger μ. In other terms, the independence of μ of the dynamical evolution reflects itself just in a linear scaling of the final density with μ. We hope to elucidate this point more thoroughly in a future work.

V. CONCLUSIONS AND PERSPECTIVES

We have proposed and discussed a simplified model for dimer compaction, with the intent to take into account relevant dynamical features, such as horizontal shaking and friction forces between particles, analyzing in detail their effects on the density time evolution. The dynamical behavior of our model is very complex with interesting features. In the absence of friction, for a single tap, the compaction dynamics cannot be interpreted as an inverse logarithmic relaxation but in terms of a stretched exponential law, which is a peculiar characteristic of a continuous range of time constants [5]. Thus, the fact that we do not find a logarithmic law but a stretched exponential relaxation could be a peculiar feature related to the single tap dynamics, since Nicodemi *et al.* [19] observe the same kind of behavior in a different model with a similar dynamics. Furthermore, we are not aware of experiments in which a single tap is applied as external perturbation, since they all refer to a tapping sequence. Actually, it turns out that the logarithmic behavior found in experiments is recovered also in our model when a sequential tapping is applied. We therefore might infer that different shaking procedures give rise to intrinsically different compaction behaviors, driven by different dynamical mechanisms. However, it still needs to be clarified whether the logarithmic law is just a good fit to the experimental data or it has a deeper meaning (see, for example, the discussion in Ref. [12]).

We also find a crossover in the behavior of the asymptotic density as a function of the shaking time with a slowing down above a critical shaking time value, indicating a possible dynamical transition process. More detailed studies of this point are planned for the future in order to reach a better understanding of the physical mechanism underlying this peculiar behavior.

Similar to what is found in experiments, horizontal shaking favors locally ordered configurations and leads to higher compaction [28,29]. We believe it would be important to address further this issue by improving our model, allowing rotations of the dimers during the dynamics.

The results obtained by introducing the frictional effect in our model indicate the important role of friction on the compaction dynamics. In particular, we find a slowing down of the dynamical behavior which is more evident in the asymptotic regime. The relaxation of the density is still described by a stretched exponential in the presence of friction, with a stretched exponent that becomes constant at large values of the friction coefficient. It would be worthwhile to explore this issue in future works with an improved modeling of the frictional force.

[1] *Granular Matter*, edited by A. Metha (Springer-Verlag, Berlin, 1994).

[2] *Physics of Dry Granular Media*, Vol. 350 of *NATO Advanced Studies Institute, Series E: Applied Science,* edited by H.J. Herrmann *et al.* (Kluwer Academic, Dordrecht, 1998).

[3] H.M. Jaeger, S.R. Nagel, and R.P. Behringer, Rev. Mod. Phys. **68**, 1259 (1996).

[4] H.M. Jaeger and S.R. Nagel, Science **255**, 1523 (1992).

[5] J.B. Knight, C.G. Fandrich, C.N. Lau, H.M. Jaeger, and S.R. Nagel, Phys. Rev. E **51**, 3957 (1995).

[6] E.R. Nowak, J.B. Knight, E. Ben-Naim, H.M. Jaeger, and S.R. Nagel, Phys. Rev. E **57**, 1971 (1998).

[7] E.R. Nowak, J.B. Knight, M.L. Povinelli, H.M. Jaeger, and S.R. Nagel, Powder Technol. **94**, 79 (1997).

[8] E. Ben-Naim, J.B. Knight, E.R. Nowak, H.M. Jaeger, and S.R. Nagel, Physica D **123**, 380 (1998).

[9] J. Talbot, G. Tarjus, and P. Viot, Phys. Rev. E **61**, 5429 (2000).

[10] S.J. Linz, Phys. Rev. E **54**, 2925 (1996).

[11] S.F. Edwards and D.V. Grinev, Phys. Rev. E **58**, 4758 (1998).

[12] J.J. Brey, A. Prados, and B. Sánchez-Rey, Phys. Rev. E **60**, 5685 (1999).

[13] K.L. Gavrilov, Phys. Rev. E **58**, 2107 (1998).

[14] P. Philippe and D. Bideau, Phys. Rev. E **63**, 051304 (2001).

[15] D.A. Head and G.J. Rodgers, J. Phys. A **31**, 107 (1998).

[16] D.A. Head, Phys. Rev. E **62**, 2439 (2000).

[17] S. Luding, M. Nicolas, and O. Pouliquen, in *Compaction of Soils, Granulates and Powders*, edited by D. Kolymbas and W. Fellin (Balkema, Rotterdam, 2000), p. 241.

[18] J.-M. Hertzsch, Eur. Phys. J. B **18**, 459 (2000).

[19] M. Nicodemi, A. Coniglio, and H.J. Herrmann, Phys. Rev. E **55**, 3962 (1997).

[20] M. Nicodemi, Phys. Rev. Lett. **82**, 3734 (1999).

[21] M. Nicodemi, Physica A **285**, 267 (2000).

[22] E. Caglioti, V. Loreto, H.J. Herrmann, and M. Nicodemi, Phys. Rev. Lett. **79**, 1575 (1997).

[23] A. Barrat and V. Loreto, J. Phys. A **33**, 4401 (2000).

[24] A. Barrat, J. Kurchan, V. Loreto, and M. Sellitto, Phys. Rev. Lett. **85**, 5034 (2000).

[25] M. Sellitto and J.J. Arenzon, Phys. Rev. E **62**, 7793 (2000).

[26] W. Kob and H.C. Andersen, Phys. Rev. E **48**, 4364 (1993).

[27] Y. Levin, J.J. Arenzon, and M. Sellitto, Europhys. Lett. **55**, 767 (2001).

[28] O. Pouliquen, M. Nicolas, and P.D. Weidman, Phys. Rev. Lett. **79**, 3640 (1997).

[29] M. Nicolas, P. Duru, and O. Pouliquen, Eur. Phys. J. E **3**, 309 (2000).

[30] F.X. Villarruel, B.E. Lauderdale, D.M. Mueth, and H.M. Jaeger, Phys. Rev. E **61**, 6914 (2000).

[31] C. Fusco, P. Gallo, A. Petri, and M. Rovere, Phys. Rev. E **65**, 026127 (2002).

[32] P.W. Kasteleyn, Physica (Amsterdam) **27**, 1209 (1961).

[33] M.E. Fisher, Phys. Rev. **124**, 1664 (1961).

[34] C. Fusco, P. Gallo, A. Petri, and M. Rovere, J. Chem. Phys. **114**, 7563 (2001).

[35] J. Duran, T. Mazozi, E. Clement, and J. Rajchenbach, Phys. Rev. E **50**, 3092 (1994).